# Toward Active Control of Limit Cycle Oscillations in an Aeroelastic Wing Using a Variable Frequency Flow Disturbance Generator

Michael T. Hughes, Daniel Hall, Ashok Gopalarathnam, and Matthew Bryant <sup>1</sup>

<sup>1</sup>Department of Mechanical and Aerospace Engineering North Carolina State University, Raleigh, NC, 27695

# **ABSTRACT**

Limit cycle oscillations (LCO) in nonlinear aeroelastic systems can be problematic for aircraft and structures, but can also be exploited for energy harvesting applications. In the presence of constant flow conditions and structural characteristics, once initiated, aeroelastic LCO can persist indefinitely. However, the introduction of external forces from impinging vortices injected upstream of the wing has been shown to modulate the self-sustaining LCO. Under the right conditions, a static bluff body placed upstream of an aeroelastic wing has been experimentally shown to annihilate pre-existing LCO and produce a cessation of oscillation. However, the exact conditions and characteristics of both the bluff body and the aeroelastic system must be tailored to produce this behavior. A rotation-oscillating cylinder with an attached splitter plate actuated by a servomotor is capable of producing a well-defined von Kármán vortex street at a range of oscillation frequencies. This system has been shown to both excite and annihilate LCO in a downstream aeroelastic wing when oscillated just below the inherent LCO frequency of the wing. Using real-time sensing on the aeroelastic wing to measure pitch angle and heave displacement, a controller can be designed to trigger the appropriate motion of the disturbance generator to inject prescribed disturbances if wing LCO are detected. The variable frequency disturbance generator can then be used to either enhance or reduce the wing LCO amplitude or cancel out the LCO entirely. The controller will be designed using state machine control theory. The state machine determines whether the wing is not in LCO, entering LCO, in LCO, or exiting LCO. In this paper, we present wind tunnel experiments that demonstrate and characterize the ability of an automatically-controlled upstream flow disturbance generator to produce or suppress LCO in an aeroelastic wing. The experiments provide insight into how controlled interactions between the aeroelastic wing and prescribed flow disturbances can be used to produce desired LCO behavior and may spur follow-on development of energy harvesting enhancement devices and on-wing disturbance generator devices that could be implemented in flight vehicles.

Keywords: aeroelasticity, limit cycle oscillations, wing-wake interaction, flow disturbance, active control

### INTRODUCTION

Aeroelasticity and its effects on structures, lifting surfaces, and other bodies has been studied extensively over the last century. Samuel Langley's prototype aircraft failed due to aeroelastic divergence [1], resulting in his loss in the race to heavier-than-air flight to the Wright Brothers who utilized wing warping effects to steer the Wright Flyer [2]. As the fledgling aviation industry continued to grow, early pioneers continued to encounter instances of aeroelastic behavior. In 1935, Theodorsen penned his foundational study, *General Theory of Aerodynamic Instability and the Mechanism of Flutter* [3], for the National Advisory Committee on Aeronautics (NACA) marking the beginning of academic study of aeroelastic phenomena. The simplest strategy to avoid the destructive effects of aeroelasticity is to design the vehicle so that the flutter speed lies beyond the range of the flight envelope. However, nonlinearities due to structural components [4,5], added external stores [6,7], and unsteady aerodynamics [8] present more complex situations which cannot always be predicted by linear flutter analysis. To address these instances of destructive aeroelasticity, a number of approaches have been taken including the addition of nonlinear energy sinks (NES) [9,10] and adaptive control of existing aircraft control surfaces [11].

In addition to aviation applications, some modern studies have explored using aeroelastic phenomena in renewable energy harvesting. Bryant and Garcia [12] proposed a system which used piezoelectric devices attached to an aeroelastic wing with degrees of freedom in pitch and heave. Further studies by Bryant and Garcia [13] built on the previous system and

experimentally characterized the power output and flutter response over a large range of freestream conditions and with both a flat plate and an airfoil. Zhao and Yang [14] showed that the addition of a beam stiffening device resulted in effective power generator for aeroelastic systems experiencing galloping instabilities, vortex-induced vibrations, and flutter. Other methods of power enhancement of such aeroelastic systems have focused on wing-wake interactions resulting from upstream bodies. Kirschmeier and Bryant [15] showed that tandem oscillating wings can be tuned to enhance the energy transfer from the wake into the downstream wing.

This paper will discuss the application of a state-machine control scheme to automatically control aeroelastic behavior in a two degree-of-freedom (2DOF) aeroelastic wing using vortices produced by an upstream variable frequency disturbance generator. The remainder of this paper will walk through the development of the aeroelastic wing and the disturbance generator experimental hardware, discuss the state-machine control scheme, present preliminary results, and discuss progress toward incorporating a recurrent neural network (RNN) machine learning model in the aeroelastic control approach.

#### METHODOLOGY

Experimental testing was performed in the North Carolina State University (NCSU) Subsonic Wind Tunnel which is a closed-return tunnel with a test section measuring 0.81 m by 1.14 m by 1.17 m. A variable pitch fan driven by a three-speed electric motor provides flow in the tunnel, measured by dynamic pressure, which is controlled by changing the blade pitch at each of the three motor speeds. The maximum dynamic pressure in the tunnel test section is 720 Pa, corresponding to a flow velocity of approximately 40 m/s at nominal temperature and atmospheric pressure.

The aeroelastic wing apparatus presented in this work was initially developed by Gianikos et al. [16] and described in more detail there and in Kirschmeier et al. [17]. The apparatus, shown in Figure 1, was comprised of the main wing section, two mounting carriages, and a support structure. The main wing section consisted of a decambered SD7003 airfoil with a chord length of 15 cm and a span of 60 cm. The wing was constructed from 3D printed ABS plastic with two internal support rods to improve the strength of the wing and reduce deflection along the span. The ends of the wing were capped with flat, elliptical plates of length 45 cm to reduce tip effects and allow to the wing section to emulate 2D flow based on the work of Visbal and Garman [18]. The mounting carriages were placed above and below the wind tunnel test section along a sliding rail mounted to the support structure. The wing section was mounted vertically in the test section and attached to the carriages via steel rods. The sliding rail allowed the wing to translate, or heave, perpendicular to the direction of flow, while bearings in the carriages allowed the wing to rotate about its mid-chord. The support structure to which the rails were attached was constructed around the wind tunnel section using T-slotted aluminum framing. No components of the support structure were attached to the wind tunnel structure to avoid any unwanted vibrations being transferred into the experimental apparatus. The elastic properties of the system were supplied by attaching linear extension springs to the mounting carriages. The extension springs providing stiffness in the heave degree of freedom were attached to either side of each carriage and a fixed point on the support structure. Springs providing stiffness in the pitch degree of freedom were mounted on the carriages themselves and attached to a pulley connected to the steel rod connecting the wing and carriage. This allowed the pitch springs to translate with the carriage as it moved along the linear mounting rail. In total eight springs were used, four for each degree of freedom split between the upper and lower carriages.

The variable frequency flow disturbance generator, shown in Figure 2, was designed to be able to produce a well-defined von Karman vortex street with shed vortices being produced at rates from less than 1 Hz to at least 8 Hz. The main body of the disturbance generator was constructed from a 10.48 cm diameter cylinder made of braided carbon fiber produced by DragonPlate<sup>TM</sup> (Elbridge, NY, USA). Research by Rockwood and Medina [19] showed that while an oscillating cylinder can produce a locked-in vortex wake with a shedding frequency equal to its oscillation frequency, the inclusion of a trailing edge splitter plate resulted in a more well-defined wake for the same range of oscillation frequencies. For this work, the splitter plate was constructed of a 1.5875 mm thick carbon fiber and birch composite material produced by DragonPlate<sup>TM</sup> (Elbridge, NY, USA) which extended one cylinder diameter from the trailing edge. The rotational axis of the disturbance generator was placed at the central axis of the primary cylinder. A SureServo SVL-210b produced by AutomationDirect (Cumming, GA, USA) was used to drive the rotation of the disturbance generator and controlled using a Copley Control (Canton, MA, USA) Xenus XTL-230-18. A maximum continuous torque of 3.3 Nm and maximum instantaneous torque of 9.9 Nm was provided by the

servomotor. While the Xenus controller provided direct control of the servomotor, an analog voltage trajectory sinusoid was supplied to the Xenus by a Keysight (Santa Rosa, CA, USA) 33500B Waveform Generator with the output controlled by the main data acquisition and control virtual instrument (VI).

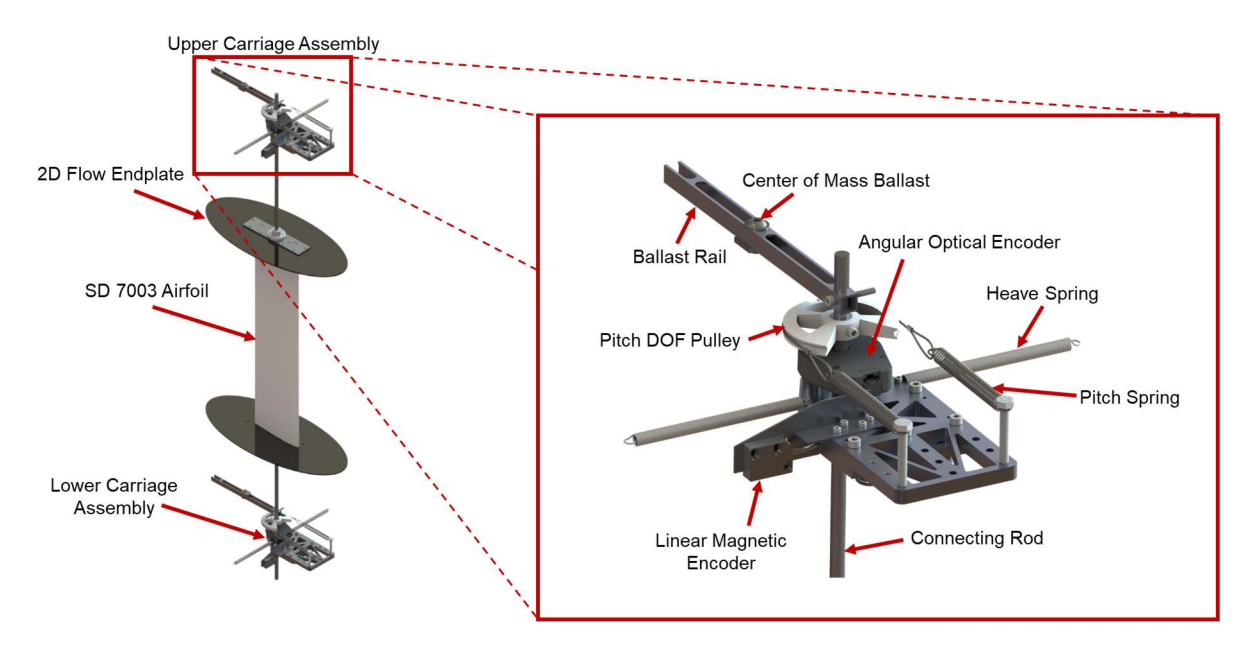


Figure 1. CAD Rendering of the aeroelastic wing apparatus showing the wing section and mounting carriages with key components labeled. The external support structure and linear rails are not shown.

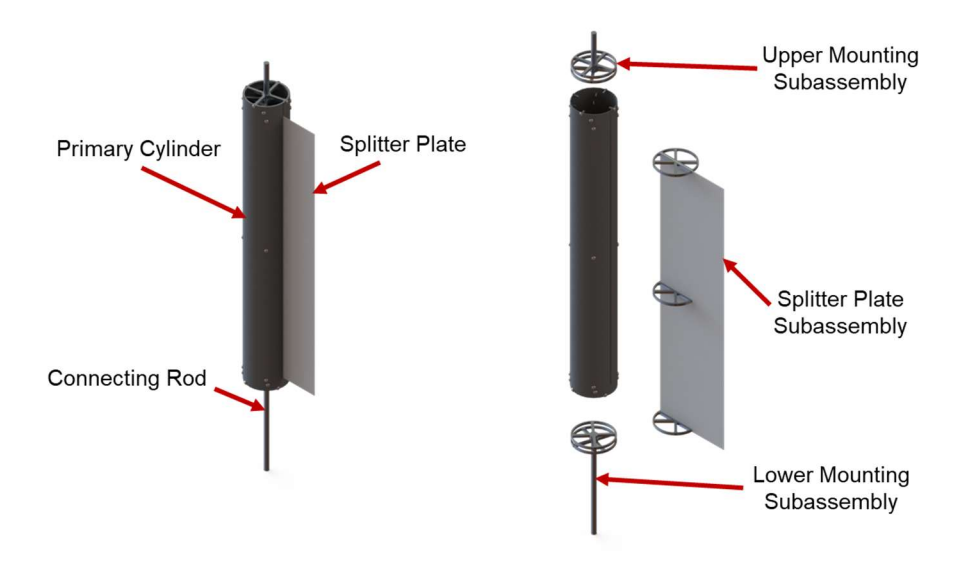


Figure 2. Fully assembled and exploded view of the variable frequency disturbance generator showing the major components and subassemblies used during construction.

National Instruments (NI) LabVIEW was run on a NI PXIe-1078 data acquisition computer and used to construct a VI to gather real-time data and control the output status of the disturbance generator trajectory. Wing pitch and disturbance generator angle were recorded with US Digital (Vancouver, WA, USA) E6-10000 optical encoders. The disturbance generator encoder was placed just above the servomotor mount and the wing encoders were place both above and below the wing and the average angle used in all calculations to mitigate effects from structural twist in the wing. Linear displacement of the wing was measured using a Renishaw (West Dundee, IL, USA) LM10 magnetic linear encoder.

Control of the disturbance generator was performed entirely within the LabVIEW VI used to run the experiment and record data. There were two methods of control used in the course of this work. The first method, User Control, allowed the researchers to manually set the oscillation amplitude and frequency and to start and stop the disturbance generator oscillation at-will. The second method, Automatic LCO Control, used preset oscillation amplitude and frequency and was started and stopped using wing pitch amplitude thresholds, allowing this control scheme to function as a rudimentary state-machine within the LabVIEW VI. An additional activation constraint was added to the Automatic LCO Control scheme based on the instantaneous wing pitch value to control the phase between the disturbance generator and wing at activation. A simplified model of the Automatic LCO Control scheme, both with and without the activation constraint, is shown in Figure 3.

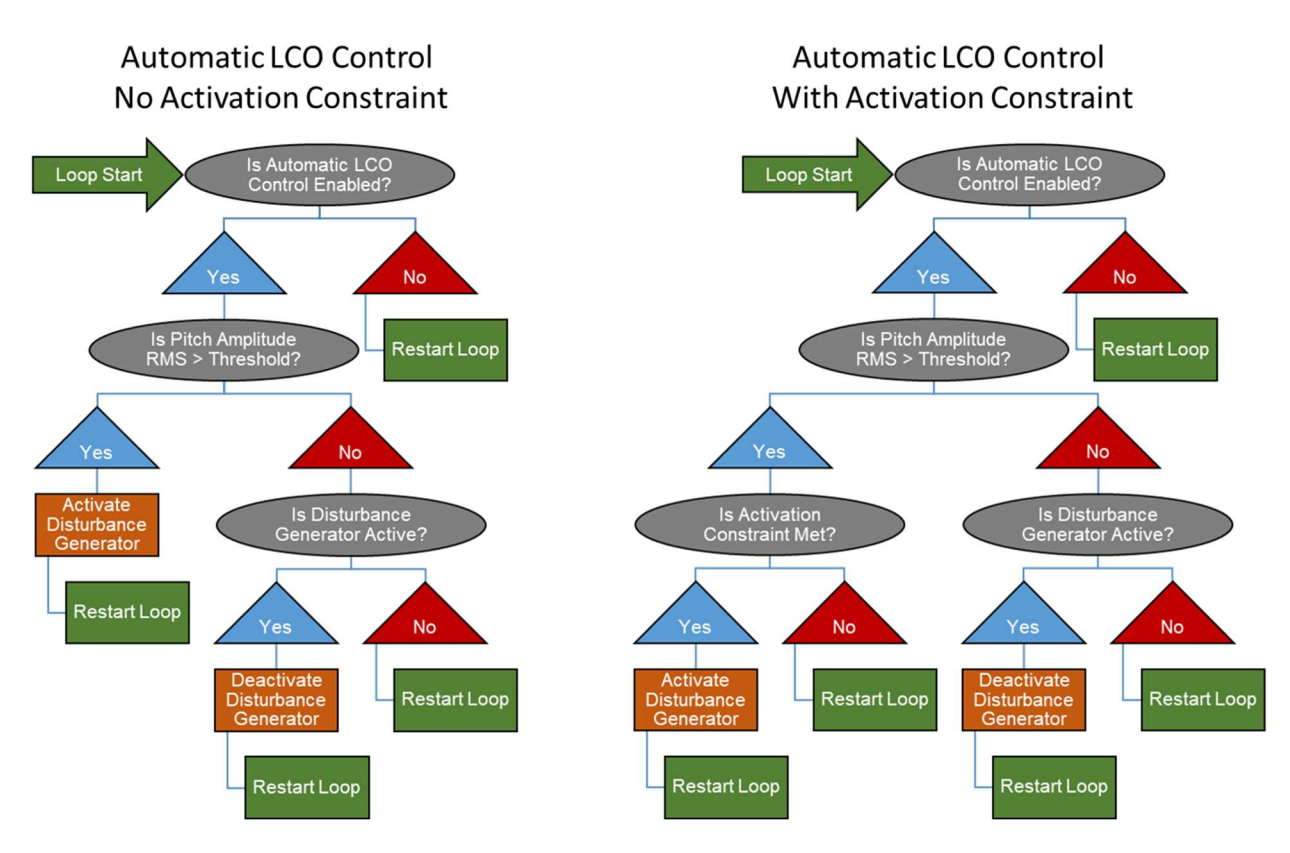


Figure 3. Decision diagrams for the Automatic LCO Control scheme used to detect and annihilate LCO in the downstream wing.

Experiments were run to test the effectiveness of the Automatic LCO Control scheme in the NCSU Subsonic Wind Tunnel. For all tests, the disturbance generator was placed at a distance of eight cylinder diameters upstream of the aeroelastic wing measured from the wing quarter-chord to cylinder central axis. Additionally, test section dynamic pressure was set to 720 Pa  $(1.0 \text{ lb/ft}^2)$ . To initially trigger LCO in the wing, researchers used the User Control scheme and oscillated the disturbance generator in a sinusoidal trajectory with a frequency of  $3.88 \text{ Hz} \pm 0.01 \text{ Hz}$ , lying just below the inherent LCO frequency of the aeroelastic wing apparatus of 3.93 Hz at this dynamic pressure, and an amplitude of approximately 25 degrees. Preset frequencies used with the Automatic LCO Control scheme to attempt LCO annihilation included 3.5 Hz, 3.7 Hz, 3.8 Hz, 4.0 Hz and 4.5 Hz, all with amplitudes of approximately 25 degrees. This range of frequencies was selected to test disturbance generator oscillation frequencies both above and below and near and far from the inherent LCO frequency.

## RESULTS AND ANALYSIS

During each test, the disturbance generator was first used to excite the aeroelastic wing apparatus with the User Control scheme. After initializing the oscillations, the wing displayed periodic amplitude growth and decay with maximum amplitude values fluctuating between approximately 0° and 50°. By stopping the disturbance generator oscillations near the peak pitch amplitude

in the wing, the system would remain at high amplitude and enter into self-sustaining LCO. This persisted until manually attenuated by reducing the freestream dynamic pressure or using the disturbance generator to annihilate the LCO. The Automatic LCO Control scheme was used to attempt annihilation in the downstream wing using disturbance generator oscillation frequencies of 3.5 Hz, 3.7 Hz, 3.8 Hz, 4.0 Hz and 4.5 Hz. The rms amplitude threshold used to stop the disturbance generator oscillations was set to 20° in all test cases. LCO annihilation was observed for all disturbance generator frequencies except the 3.5 Hz and 4.5 Hz cases. Disturbance generator oscillation frequencies of 3.8 Hz resulted in time-to-annihilation (TTA) values ranging from 13.34 seconds to 19.375 seconds as shown in Table 1. Figure 4 provides an example of the pitch and heave time histories of one such test.

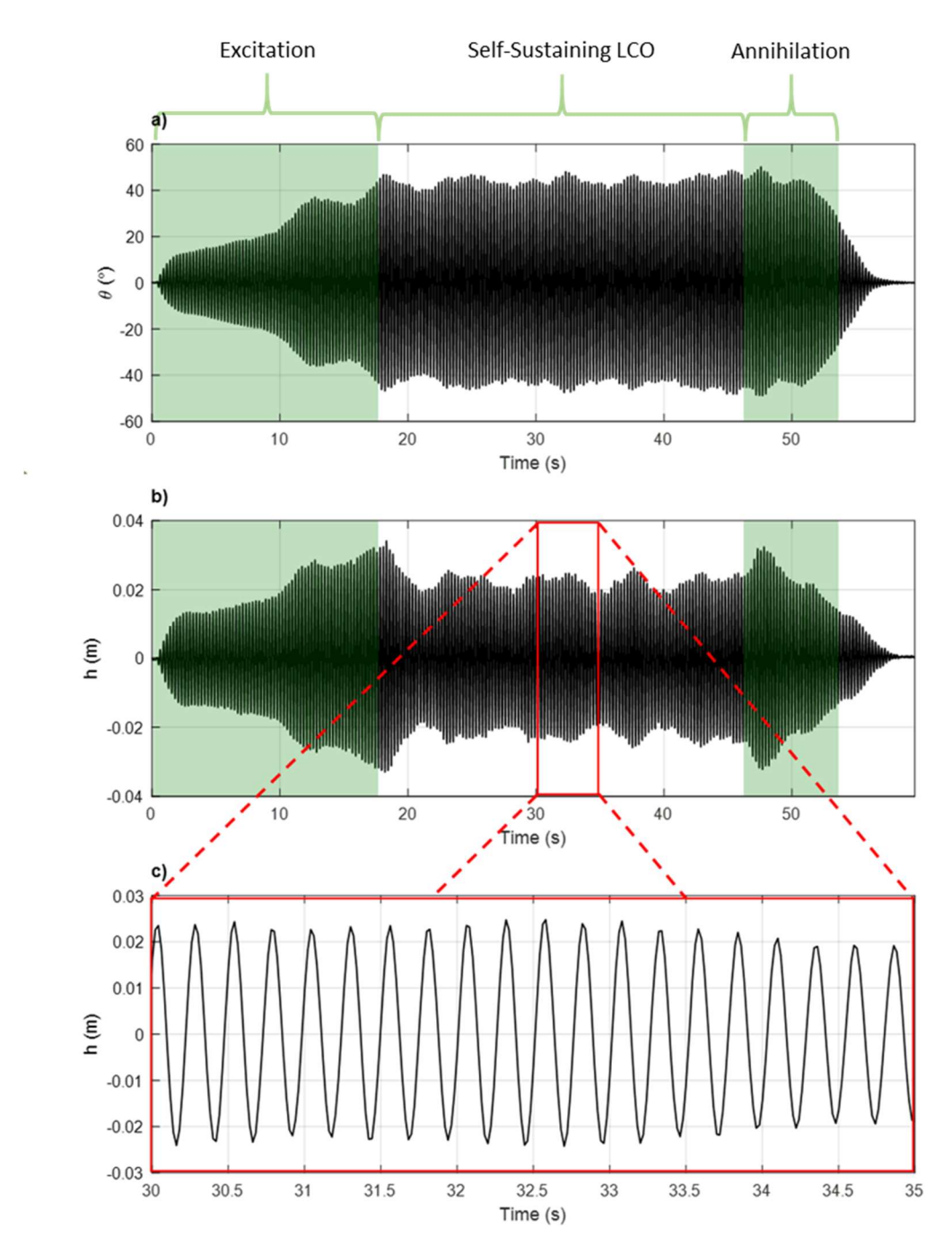


Figure 4. Time histories for a) pitch, b) heave, and c) zoomed-in heave for an Automatic LCO Control test with the disturbance generator frequency set to 3.8 Hz. The green shaded areas represent time when the disturbance generator oscillations are active.

Following the initial tests to verify that the Automatic LCO Control scheme could successfully annihilate pre-existing LCO in the downstream wing, additional constraints were added to the disturbance generator activation conditions. Using the instantaneous wing pitch angle, an activation constraint was applied to force a defined phase difference between the disturbance generator and the downstream wing. The first constraint required that the instantaneous wing pitch must be greater than 30 degrees while the second activation constraint required an instantaneous wing pitch angle between -5 degrees and 5 degrees. For these tests, disturbance generator frequencies of both 3.8 Hz and 4.0 Hz were used to annihilate LCO. As shown in Table 1, TTA ranged from 7.40 seconds to 20.16 seconds, with the shortest average TTA found when the oscillation frequency was set to 4.0 Hz and the activation constraint requiring wing pitch greater than 30 degrees.

Table 1. Results from test cases which resulted in successful LCO annihilation.

Test Number	Disturbance Generator Frequency	Instantaneous Wing Pitch Activation Constraint	Time to Annihilation
1	3.8 Hz	-	15.15 s
2	3.8 Hz	-	19.38 s
3	3.8 Hz	-	15.91 s
4	3.8 Hz	-	13.75 s
5	3.8 Hz	-	13.34 s
6	3.7 Hz	-	7.98 s
7	3.8 Hz	$\theta > 30^{\circ}$	16.96 s
8	3.8 Hz	$\theta > 30^{\circ}$	12.84 s
9	4.0 Hz	$\theta > 30^{\circ}$	12.10 s
10	4.0 Hz	$\theta > 30^{\circ}$	7.40 s
11	3.8 Hz	$-5^{\circ} < \theta < 5^{\circ}$	17.02 s
12	3.8 Hz	$-5^{\circ} < \theta < 5^{\circ}$	7.86 s
13	4.0 Hz	$-5^{\circ} < \theta < 5^{\circ}$	20.16 s
14	4.0 Hz	$-5^{\circ} < \theta < 5^{\circ}$	19.06 s

Spectral analysis on the wing pitch and heave motion was performed using MATLAB's Fast-Fourier Transform (FFT) tool. The results from the FFT performed on the wing response when the disturbance generator was annihilating the LCO show a relationship between the difference in pitch and heave frequency and TTA, as seen in Figure 5. For the tests with the shortest TTA, the difference between the pitch and heave frequencies is large, whereas the opposite is true for tests with longer TTA. Additionally, it is important to note that the three tests with the fastest TTA each represent a different disturbance generator oscillation frequency (3.7, 3.8, and 4.0 Hz) suggesting that the disturbance generator oscillation frequency is not directly responsible for the reduced TTA. These three cases also show both pitch and heave frequencies below the inherent LCO frequency (i.e. the oscillation frequency when the wing is exhibiting LCO while the disturbance generator is stationary).

# PLANNED FUTURE WORK

To further develop the controller for the disturbance generator and oscillating wing system, the use of machine learning models is being explored. Specifically, a recurrent neural network (RNN) is being developed to take in time history data from these wind tunnel experiments and learn the system's behavior. Due to their architecture, RNNs can utilize the time history dependency of data to recognize the trends in the response of a system, as was shown by Chen et al. [20]. This group utilized a type of RNN known as a long short-term memory (LSTM) neural net to predict wind speeds and flow [20]. A simple RNN model schematic can be seen in Figure 6. RNNs function similarly to other neural networks by taking in the input vector x for each time step, applying matrix transformations on the input vector in the hidden layer h, and generating a predicted output y.

Unlike other neural networks, though, RNNs "remember" the hidden layer of the previous time step to be used as another input for the current time step, thus allowing them to identify time history trends.

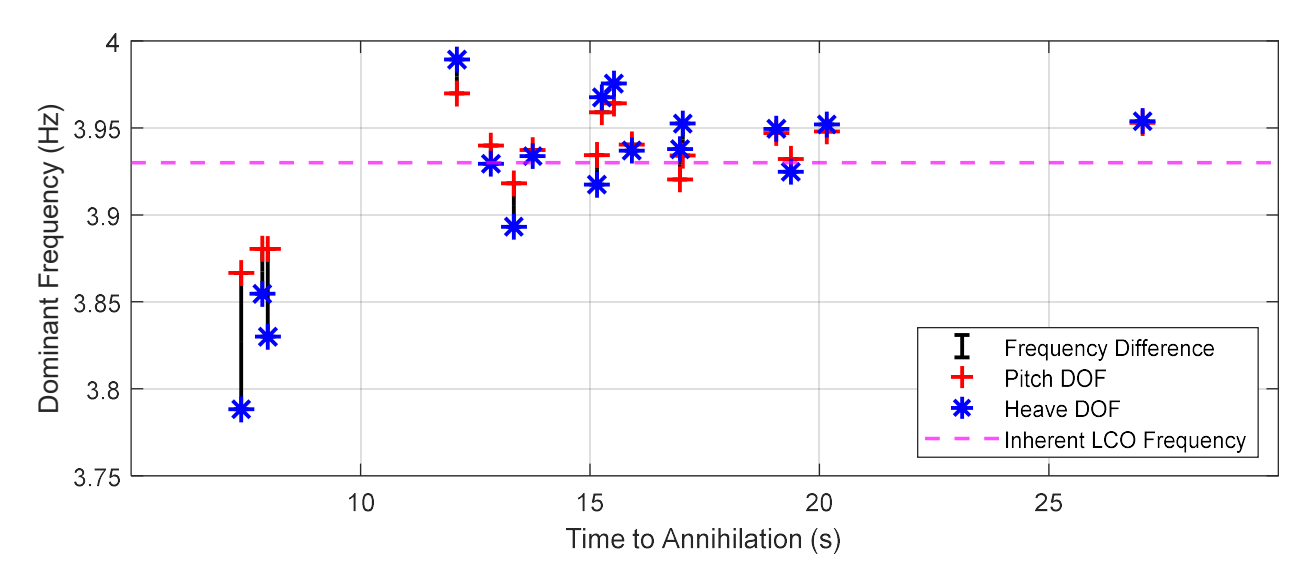


Figure 5. Dominant frequency during LCO annihilation found using FFT on the pitch and heave response in the wing. Larger gaps between the pitch and heave frequencies appear to reduce the TTA.

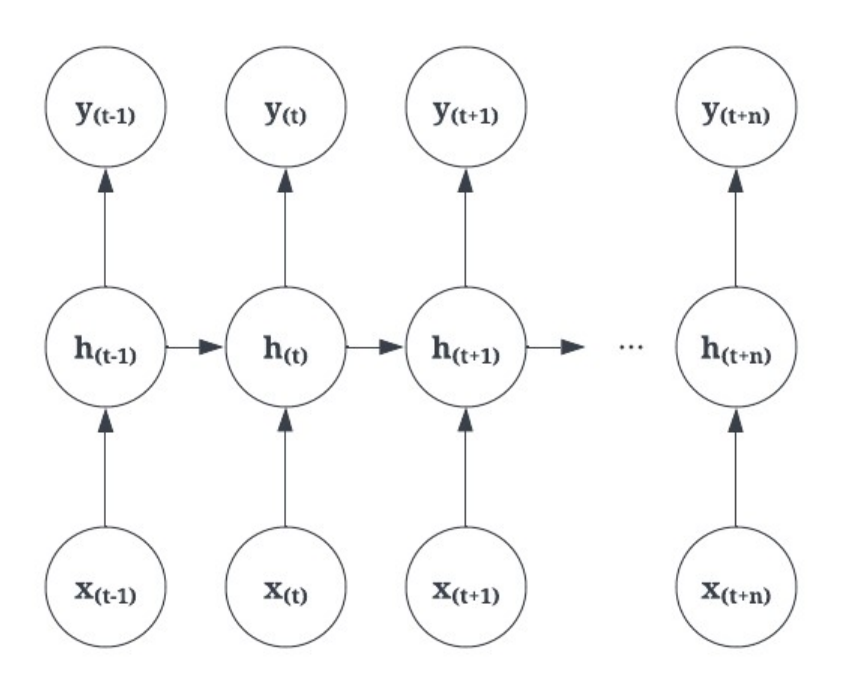


Figure 6. Schematic of a basic recurrent neural network model, which evaluates the function output at each time step and utilizes the hidden layers from the previous time step in the current time step's calculation.

In order to proceed with training the model, he aeroelastic data from the wind tunnel tests had to be analyzed and prepared to feed to the model. Specifically, this meant labeling each dataset with the appropriate states of buffeting, growth, decay, and LCO. To do so, the envelope of the pitch amplitude was observed, and the critical points of that curve were calculated. These data points were then divided into four groups using the statistical method of k-means clustering, which utilizes a randomized

group of n centroids to divide the data points based on proximity. These four groups were then used to label their associated states. Since the states weren't always sequential, it was important to make sure the model will have a uniform chance of selecting each state; therefore, a one-hot encoding method was used so that there would be a uniform distance between each state vector. Rather than labeling the data with numerical states 1-4 for buffeting-LCO, this method uses unit vectors to label the data. As such, the labeling for each data point consisted of an appended vector of [1, 0, 0, 0] for buffeting, [0, 1, 0, 0] for growth, [0, 0, 1, 0] for decay, and [0, 0, 0, 1] for LCO. Using k-means to cluster the data showed that some similarities exist between the growth and LCO regions, as the upper portion of the growth regions is grouped into the LCO label. This agrees with the experimental results, as manual LCO excitation via controlling the disturbance generator occurs most consistently in this higher amplitude portion of the growth region. A full labeled time history of the wing pitch can be seen in Figure 7, showing the grouping of high amplitude growth with LCO. With the labeled data, the RNN model can be trained and its hyperparameters tuned to accurately predict outcomes for the updated controller.

Once the neural network is fully trained, it will be implemented into the controller in place of the amplitude cutoff in the current state machine. The trained RNN will read in the wing motion data in real-time, allowing it to identify the state of the system and forecast the control action needed to drive the wing to the desired LCO behavior more quickly. The controller will utilize the RNN for a two-fold purpose of increasing the efficiency of LCO excitation and annihilation. Specifically for the process of annihilation, the controller will take in the initial wing response during LCO via the rotary and linear encoders, and then feed the data to the neural network model. This planned implementation method for the RNN in the controller is shown below in Figure 8. Next, the RNN will predict whether or not and when the wing's response is trending towards decay, which will indicate the optimal time to begin the annihilation procedure. If it predicts the desired behavior, the disturbance generator will be activated so that the wing LCO can be canceled out, returning the wing to equilibrium in the same fashion as the current state machine. Otherwise, the disturbance generator remains inactivate until the decay state is predicted.

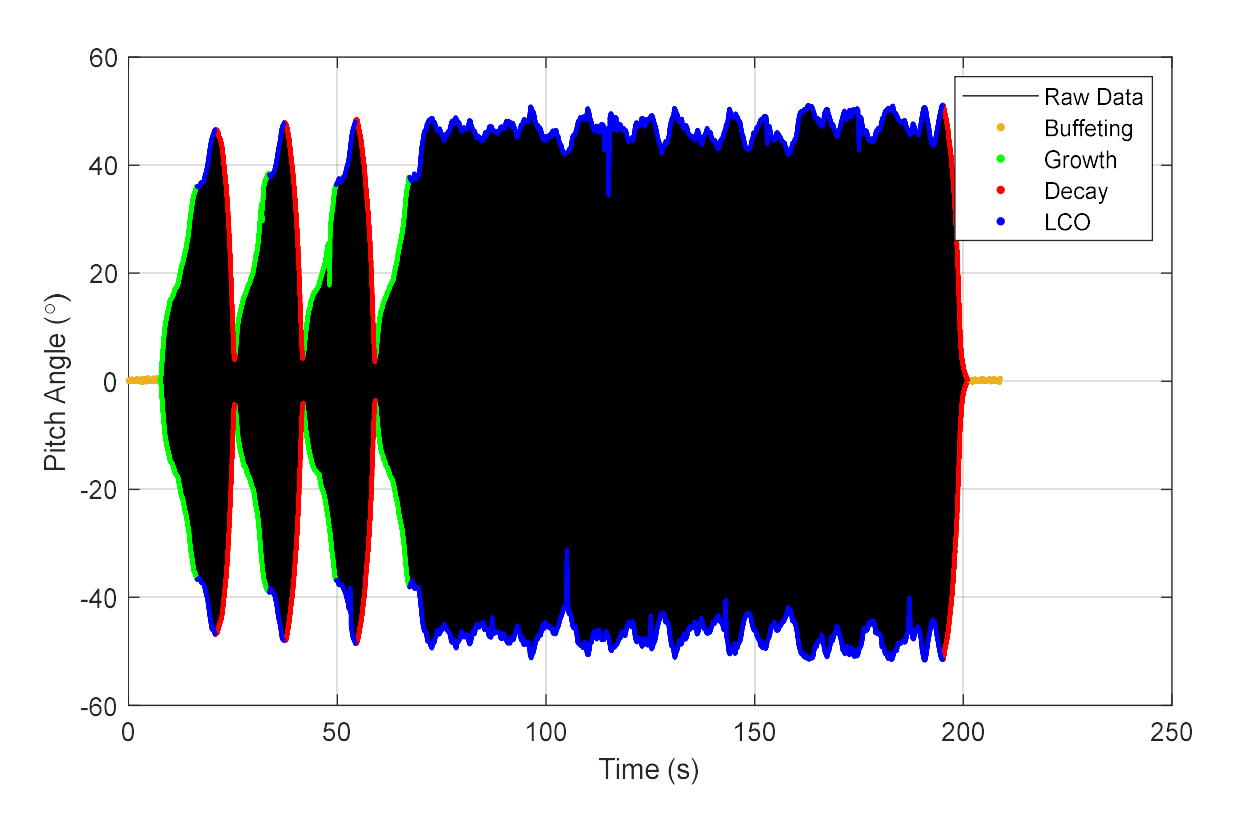


Figure 7. Labeled data for a test case with disturbance generator frequency of 3.87 Hz. The yellow regions denote the buffeting label in the envelope curve, green denotes growth, red denotes decay, and blue denotes LCO.

#### CONCLUSIONS

This paper has shown that a state-machine control scheme can be used with a variable frequency flow disturbance generator to automatically control limit cycle oscillations (LCO) in a two degree-of-freedom (2DOF) aeroelastic wing. In its current form, the control scheme uses preset oscillation frequencies near the inherent LCO frequency of the aeroelastic wing to annihilate preexisting LCO. However, moving forward, the disturbance generator oscillation frequency could be set as a variable based on real-time sensing of the wing LCO frequency and coupled with a feedback control scheme to drive the time to annihilation (TTA) towards zero. Additionally, the researchers have begun to investigate the use of a recurrent neural network (RNN) model to identify the real-time state of the system. This could be used alongside the existing control scheme to forecast LCO before the wing begins exhibiting large-amplitude oscillation. Coupled with the RNN, the controller could be tuned to drive the wing to the desired LCO behavior more quickly.

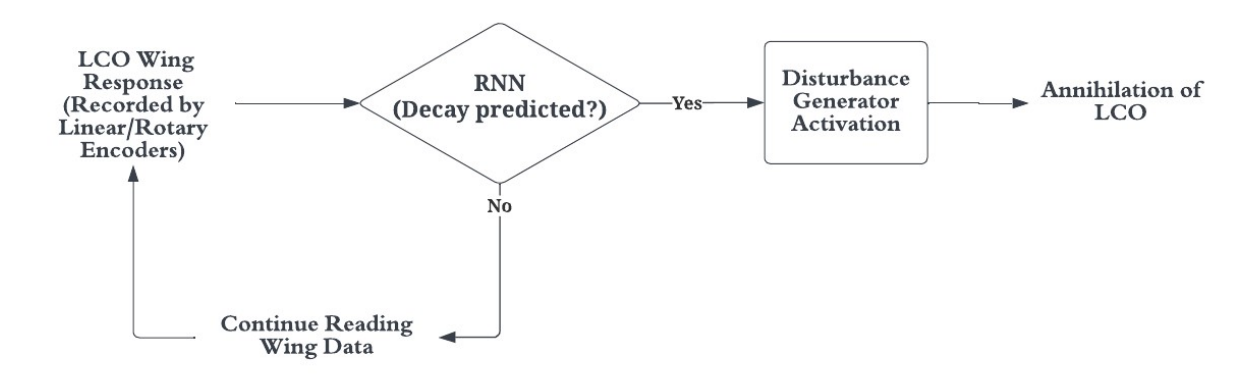


Figure 8. Simple block diagram for the controller with implemented RNN model used to annihilate LCO in the downstream wing.

## **FUNDING SOURCES**

Funding for this research is provided by the National Science Foundation for its financial support of this study under Award No. CMMI-2015983 which is managed by Dr. Robert Landers.

# **ACKNOWLEDGEMENTS**

The authors would like to thank Dr. Shreyas Narispur and Dr. Mingtai Chen for their guidance and training on operation of the NCSU Subsonic Wind Tunnel and undergraduate student Ethan Sites for his preparation of testing hardware and tunnel operation.

#### REFERENCES

- [1] Garrick, I. E., and Reed, W. H., "Historical Development of Aircraft Flutter," *Journal of Aircraft*, Vol. 18, No. 11, pp. 897-912, 1981.
- [2] Ricketts, R. H., "Experimental Aeroelasticity History, Status and Future in Brief," NASA Technical Report, TM-102651, April 1990.
- [3] Theodorsen, T., "General Theory of Aerodynamic Instability and the Mechanism of Flutter," Tech. Rep. 496, NACA, 1935.
- [4] Patil, M. J., and Hodges, D. H., "On the importance of aerodynamic and structural geometrical nonlinearities in aeroelastic behavior of high-aspect-ratio wings," *Journal of Fluids and Structures*, Vol. 19, pp. 905-915, 2004.
- [5] O'Neil, T., Gilliatt, H., and Strganac, T. W., "Investigations of aeroelastic response for a system with continuous structural nonlinearities," Proc. AIAA 37<sup>th</sup> Structure, Structural Dynamics and Materials, April 1996.
- [6] Goodman, C., Hood, M., Reichenbach, E., and Yurkovich, R., "An Analysis of the F/A-18C/D Limit Cycle Oscillation Solution," 44th AIAA/ASME/ASCE/AHS/ASC Structures, Structural Dynamics, and Materials Conference, 2003.
- [7] Hayes, W. B., and Sisk, K., "Prevention of External Store Limit Cycle Oscillations on the F/A-18E/F Super Hornet and EA-18G Growler Aircraft," Tech. Rep. RTO-MP-AVT-152, North Atlantic Treaty Organization/Science and Technology Organization, 2008.
- [8] Dowell, E. H., and Tang, D., "Nonlinear Aeroelasticity and Unsteady Aerodynamics," *AIAA Journal*, Vol. 40, No. 9, pp. 1697-1707, September 2002.
- [9] Pidaparthi, B., and Missoum, S., "Stochastic Optimization of Nonlinear Energy Sinks for the Mitigation of Limit Cycle Oscillations," *AIAA Journal*, Vol. 57, No. 5, 2019, pp. 2134–2144.
- [10] Bichiou, Y., and Hajj, M. R., "Effectiveness of a Nonlinear Energy Sink in the Control of an Aeroelastic System," *Nonlinear Dynamics*, Vol. 86, 2016, pp. 2161–2177.
- [11] Strganac, T. W., Ko, J., Thompson, D. E., and Kurdila, A. J., "Identification and Control of Limit Cycle Oscillations in Aeroelastic Systems," *Journal of Guidance, Control, and Dynamics*, Vol. 23, No. 6, pp. 1127-1133, November-December 2000.
- [12] Bryant, M., and Garcia E., "Development of an Aeroelastic Vibration Power Harvester," Proc. SPIE 7288, Active and Passive Smart Structures and Integrated Systems, April 2009.
- [13] Bryant, M., and Garcia E., "Energy Harvesting: a Key to Wireless Sensor Nodes," Proc. 7493, Second International Conference on Smart Materials and Nanotechnology in Engineering, October 2009.
- [14] Zhao, L., and Yang, Y., "Enhanced Aeroelastic Energy Harvesting with a Beam Stiffener," *Smart Materials and Structures*, Vol. 24, No. 3, 2015.
- [15] Kirschmeier, B., and Bryant, M., "Experimental Investigation of Wake-Induced Aeroelastic Limit Cycle Oscillations in Tandem Wings," *Journal of Fluids and Structures*, Vol. 81, pp. 309-324, 2018.
- [16] Gianikos, Z. N., Kirschmeier, B. A., Gopalarathnam, A., and Bryant, M., "Limit Cycle Characterization of an Aeroleastic Wing in a Bluff Body Wake," *Journal of Fluids and Structures*, Vol. 95, 2020, p. 102986.
- [17] Kirschmeier, B. A., Gianikos, Z., Gopalarathnam, A., and Bryant, M., "Amplitude Annihilation in Wake-Influenced Aeroelastic Limit-Cycle Oscillations," *AIAA Journal*, Vol. 58, No. 9, 2020, pp. 4117–4127.
- [18] Visbal, M. R., and Garmann, D. J., "Numerical Investigation of Spanwise End Effects on Dynamic Stall of a Pitching NACA 0012 Wing," Proc. 55th AIAA Aerospace Sciences Meeting, January 2017.
- [19] Rockwood, M., and Medina, A., "Controlled Generation of Periodic Vortical Gusts by the Rotational Oscillation of a Circular Cylinder and Attached Plate," *Experiments in Fluids*, Vol. 61, No. 3, 2020.
- [20] Chen, Y., Zhang, S., Zhang, W., Peng, J., Cai, Y. "Multifactor spatio-temporal correlation model based on a combination of convolutional neural network and long short-term memory neural network for wind speed forecasting", *Energy Conversion and Management*, Vol. 185, pp. 783-799, 2019